

TUNING AND FIELD MEASUREMENT TECHNIQUES IN A RESONANTLY
COUPLED ACCELERATOR TANK*

L. N. Engel and E. A. Knapp
Los Alamos Scientific Laboratory
Los Alamos, New Mexico

Introduction

Long $\pi/2$ mode side coupled cavity chains have been shown^{1,2} to have excellent properties for use as standing wave accelerator structures. Very loose mechanical tolerances, coupled with very high shunt impedance and electrical stability have been predicted for long chains of this type. In this report we discuss the tuning and measurements made on a long cavity chain designed to check the predictions of the theory and develop fabrication and tuning techniques useful for mass production of cavity chains of this type. An 805 MHz, side-coupled, 39 accelerating cell, experimental model was fabricated and tuned. Designed to have a constant phase velocity of 0.65 speed of light, this tank was the first accurately fabricated side-coupled cavity chain of any appreciable length studied so far. The results of the study on this model showed that the predictions of the equivalent circuit analysis for $\pi/2$ mode structures were verified in all cases where direct experimental tests were feasible; an economical and practical method of tank fabrication was developed; and tuning techniques adaptable to the mass production of long tanks were devised.

Final results of the low power tuning as shown in Table I indicate that the tank has a resonant frequency of 804.910 MHz for the $\pi/2$ mode, a stop band of 19.2 kHz, a shunt impedance ZT^2 of 28.9 M Ω /m, and a maximum electric field variation of $\pm 1.2\%$ within the tank. The phase shift from one end to the other was essentially zero.

The finished cavity chain prior to final tuning and installation of vacuum and cooling systems is shown in Fig. 1. The particle velocity is equal to the electromagnetic wave velocity if the length of the cavity is $\beta\lambda/2$. There will be N normal modes of oscillation, each distinguished by a discrete eigenvalue or frequency, for a chain of N cavities. This is due to the fact that there are N possible ways a travelling wave can propagate through the chain and return to reinforce itself at a starting point.

The coupling strength between the cavities determines the frequency separation between the zero and π modes. One must have strong coupling in order to have large band width or mode separation. This side-coupled model achieves magnetic coupling through small slots in the common wall between coupling and accelerating cell cavities. In this model, with the drive at the center, the mode separation is approximately 1.4 MHz.

Table I

Final Parameters of Side-Coupled
Experimental Model

Number of accelerating cells - 39
Number of coupling cells - 38
Drive cell is accelerating cell 20
 $\beta = 0.649$ @ $f = 804,900$ MHz

Typical proton energy gain = 1.25 MeV/m for meson factory service
Length of one accelerating cell = 4.764 in.
 $\pi/2$ frequency of accelerating cells = 804.910 MHz @ 72 F, no vacuum
Coupling cell frequency = 802.844 MHz
Coupling between accelerating cell and nearest coupling cell = 4.17%
Coupling between accelerating cells = -0.93%
Coupling between coupling cells = 0.52%
Stop band = 19.2 kHz
Shunt impedance $ZT^2 = 28.9$ M Ω /m
Unloaded Q of assembled tank = 17,800
Transit time factor = 0.83
Voltage Standing Wave Ratio in the waveguide driving the tank = 1.075
Coupling coefficient = 0.93 (undercoupled)
Electric field variations = $\pm 1.2\%$
Average phase shift from one accelerating cell to another $< 0.3^\circ$
Total phase shift of tank from end to end $< 0.2^\circ$

Frequency Tuning Techniques on
the Individual Cells

The resonant frequency of the individual cells was changed by altering the capacitive or inductive loading within that cavity. Referring to Fig. 2, the frequency of the accelerating cell was increased if gap H was increased. The resonant frequency was decreased if the diameter D was increased. The electric field within the cavity was maximum at the location of radius R on the "drift tube" as shown in the figure. Small dimensional changes in R altered the resonant frequency considerably. The resonant frequency of the side-coupled cell was similarly regulated through alteration of coupling cell gap G.

The usual tuning procedure for the individual cells was to place the machined segment with its coupling cell between two flat plates. Sufficient pressure was then brought to bear upon the plates, insuring positive metal-to-metal contact without warping the plates. With the use of a sweep signal generator and oscilloscope, the three expected modes (0, $\pi/2$, π) produced by this arrangement were then visible. If all the modes were not present, which is common when the frequencies are widely different, one could have found the coupling cell frequency by inserting a drive and receiving probe within the coupling cell proper with the segment sitting on a non-metallic surface, such that only the coupling cell would resonate. Since the required dimensional change was probably great, the relative effect of the perturbation of the resonant frequency due to the presence of the probes and slightly incorrect boundary conditions was small.

It was usual to fabricate the drift tubes of the segment and bosses of the coupling cells extra long so that the initial $\pi/2$ frequency would be lower than the ultimate $\pi/2$ frequency. Metal was

removed from the drift tubes and the coupling cell according to empirical cutting curves as shown in Fig. 3. The results indicated a cutting slope of 5.2 mils/MHz on the drift tubes and 2.4 mils/MHz in the coupling cell gap for this particular model. The discontinuity in the drift tube curve was believed to be due to an accidental adjustment on the radius mentioned previously. We found that on the whole the cells could be tuned to ± 50 kHz, thus providing an option for the interchange of segments in assembling a cavity chain.

Tuning Techniques for the Coupling Cells

The tuned up cavity chain also called for the coupling cell frequency to be equivalent to the accelerating cell frequency, taking into account the coupling constants. That is, to have no stop band at the $\pi/2$ mode in the dispersion curve for the structure. The resulting effect was to maximize the Q of the structure since minimization of the field in the coupling cells reduced the power losses in the coupling cells, and to minimize effects due to frequency errors in individual cells. Consequently, the effective shunt impedance was maximized for a particular accelerator structure.

A computer program utilizing a least squares fit to the theoretical dispersion expression for a cavity chain had been developed. This program could calculate the coupling cell frequency for a chain of resonators with nearest neighbor and next nearest neighbor coupling. Five parameters were needed for the fit, the three coupling constants, and the accelerating and coupling cell frequencies. Since five parameters were involved, one needed at least five data points, i.e., five frequencies for five mode numbers. The more data available, the more reliable the fit. Several segments with their coupling cells were usually stacked and the frequencies of the modes present were measured. Figure 4 shows examples of the fit of the dispersion curve for a multi-cell system. In the first case the frequencies of the coupling cells are not equivalent to that of the accelerating cells taking into account the next nearest neighbor coupling. The discontinuity or stop band in the curve corresponds to this difference in frequency. The figure on the right shows the continuous dispersion curve obtained when the two frequencies were properly adjusted.

Frequency Adjustment Due to Multicell Stacking

The $\pi/2$ mode frequency of a multicell stack was lower than that of a single two halfcell cavity system due to the symmetry conditions at the reflecting plane since the two halfcell cavity chain appeared to be an infinite chain with the coupling cavity on one side only. As a stack was made of these cavities the change in frequency of the $\pi/2$ mode $\delta f = \langle f_1(\pi/2) \rangle - f_s(\pi/2)$, $N = 2, 3, 4, \dots$, asymptotically approached the value for an infinite stack as shown in Fig. 5, where $\langle f_1(\pi/2) \rangle$ is the mean of the $\pi/2$ mode frequencies of the cells measured individually, and $f_s(\pi/2)$ is the $f(\pi/2)$ of all the cells measured as a single cavity chain. It is this δf which was used in the

determination of the individual cell frequency in order that the desired chain frequency may be obtained. As an example, inspection of Fig. 5 shows that a tuned cavity chain for 805 MHz would require that the individual two half cell system be tuned to 805.318 MHz if thermal and vacuum effects on the frequency were ignored.

Tuning the end cells consisted of adjusting the end cell $f(\pi/2)$ such that it matched the $f(\pi/2)$ of an interior cavity of an infinite chain. This was done by placing two properly tuned segments with their coupling cells between two end cells and driving the system at the $f(\pi/2)$ obtained from the multicell stacking. One assumed that the drift tube dimensions of the end cells were similar. The electric field in the coupling cells was then minimized by adjusting the drift tubes on the end cells. The results of the tuned end cells with a long stack are shown in Fig. 5. The tuning was not perfect for this model, but adequate for our purposes.

Frequency Adjustment Due to Thermal and Vacuum Effects

Our experimental data indicated that there was a frequency increase of 165 kHz due to the presence of 10^{-4} torr vacuum, and a 7.65 kHz/°F decrease due to the difference in the cavity chain operating temperature with individual cell tuning temperature.

There is also a frequency decrease on the order of several hundred kHz due to the temperature gradients set up when the cavity is excited by high power high duty factor rf. Data on this effect was not available at the time we tuned the model.

$$\text{Thus, } \langle f_1(\pi/2) \rangle_{72^\circ} = f_{op}(\pi/2) - \alpha \delta T - \delta f_v + \delta f_a$$

where

$$\langle f_1(\pi/2) \rangle_{72^\circ} \text{ was the individual cell frequency with flat plate termination tuned at room temperature,}$$

$$f_{op}(\pi/2) \text{ was the desired } f(\pi/2) \text{ at operational temperature,}$$

$$\alpha \delta T \text{ was the product of } -7.6 \text{ kHz/}^\circ\text{F and the difference in the tuning temperature and operational temperature,}$$

$$\delta f_v \text{ was the } 164.4 \text{ kHz increase due to evacuation,}$$

$$\delta f_a \text{ was the multicell asymptote factor.}$$

Each individual cell was tuned to as close to 805.138 MHz as possible (± 50 kHz). Under an operational temperature of 90° this would have given a $f(\pi/2)$ of 804.748 MHz. At low power (1 watt) at 72° F and not evacuated the tank should have resonated at 804.720 MHz. When the tank was brazed and assembled, it resonated at 804.720 MHz. The point to be made is that it seems possible under production conditions, to tune a tank's frequency very close to a predicted value during the machining stage without too much effort.

Tank-to-Waveguide Impedance Matching

Power was coupled into the tank through an aperture in accelerating cell 20 as shown in

Fig. 6. The iris diameter was cut to match the tank impedance to that of the waveguide. With the tank slightly under-coupled, the final VSWR after tuning was 1.075. Initially the iris was 2.5 inches in diameter. With meticulous cutting the iris was enlarged to an oval having a major axis of 4.3 inches. Due to the presence of such a gap, the center cell was considerably detuned. The gap between the drift tubes was enlarged approximately 0.070 in. to bring this cell back to the frequency of its neighbors. The additional gap caused a small reduction in the peak electric field in cell 20 as shown in Fig. 7. Both the unloaded Q of the coupling coefficient were determined through observation of the input VSWR and the voltage minimum position along a slotted waveguide. This method is discussed in Ginzton.³

Reduction of Tilt of Electric Field

Figure 7 illustrates the frequency perturbation due to a 0.375-inch round brass bead drawn down the beam axis of the tank before the final tuning process. Since the electric field is proportional to the square root of frequency change, the figure shows that the electric field had a tilt of $\pm 4.5\%$. Looking at individual cell frequencies by shorting out the nearest coupling cells, it was determined that the individual cell frequencies were within ± 500 kHz of each other after several brazing operations were undertaken in assembling the tank. Our equivalent circuit analysis⁴ has indicated that ± 500 kHz frequency errors would result in a small shunt impedance reduction and field unflatness; this field unflatness is seen in Fig. 7. The tuning procedure described earlier,^{1,4} which consisted of tuning accelerating cell frequencies to minimize coupling cell fields, was used to flatten the tank, and also simultaneously to raise the tank frequency to the desired frequency of 804.900 MHz. Approximately a foot of 3/16-inch ball chain was placed in each accelerating cell until the tank resonated at 804.900 MHz. Driving the tank through cell 20 at 804.900 MHz, the electric field in coupling cell one was measured with an electric probe. If the field in the coupling rose as the chain was removed from accelerating cell one, then the frequency of the accelerating cell was raised by perturbing the cell with a special circumferential vise until the field in the coupling cell was a minimum. This procedure was repeated down the tank until the drive cell was reached. Then one moved to cell 39 and repeated the process. Figure 8 shows that the tilt in the electric field was reduced to $\pm 1.2\%$. The residual tilt was associated with slot dimension errors. One should also note in the figure that the mechanical rf joints had negligible effect on the field within their cells.

Coupling Cell Electric Field Measurements

A plot of the electric fields in the coupling cells, measured with an electric probe is shown in Fig. 9. This field shows the expected linear dependence on cell number.⁴ The ratio of the energy stored in the accelerating cell was difficult to measure directly but appeared to agree qualitatively with the expected value.

Phase Measurement

The average phase shift from one accelerating cell to another was less than 0.3° . Maximum phase shift between any two accelerating cells was 1.36° . End to end phase shift was less than 0.20° . The equipment that was used has a resolution of approximately $\pm 0.5^\circ$. One could say then that the phase shift between accelerating cells was essentially zero within the limits of the measuring device.

Conclusions on Tank Behavior

Some of the conclusions which may be drawn from the behavior of this model so far are:

1. The predictions of the equivalent circuit analysis carried out for the $\pi/2$ mode structures have been verified in all cases where direct experimental tests are feasible.¹ In particular, the great tolerance to mechanical error in the $\pi/2$ mode has been verified.²
2. An economical and practical method for fabricating accelerator cavities of this type was developed, including an effective demountable rf joint which allows production in short lengths.
3. With some improvements, the tuning techniques as outlined in this paper are adaptable to the mass production of side-coupled cavity chains.

Acknowledgments

The work reported is the result of a joint effort of many people. The success of the fabrication program was primarily due to the efforts of H. G. Worstell and V. E. Hart. R. J. Bueschel, W. H. Yeamans, W. E. Smith, and J. W. Haskins did an excellent job in machining the model. C. E. Manger and W. L. Jennings contributed greatly to the tuning.

References

1. E. A. Knapp, "800 MeV RF Structures," Proc. of the MURA Conf. on Linear Accelerators, Stoughton, Wisconsin, July 20-24, 1964, p. 55-57. Available from U.S. Dept. of Commerce, Springfield, Va., TID-4500.
2. E. A. Knapp, et al, "Accelerating Structures for High Current Proton Linacs," IEEE Trans. on Nucl. Sci., NS-12, p. 162.
3. Ginzton, E. L., Microwave Measurements, McGraw Hill, 1957, p. 405-407, 414-416.
4. E. A. Knapp, et al, loc. cit., p. 160.

* Worked performed under the auspices of the U. S. Atomic Energy Commission.

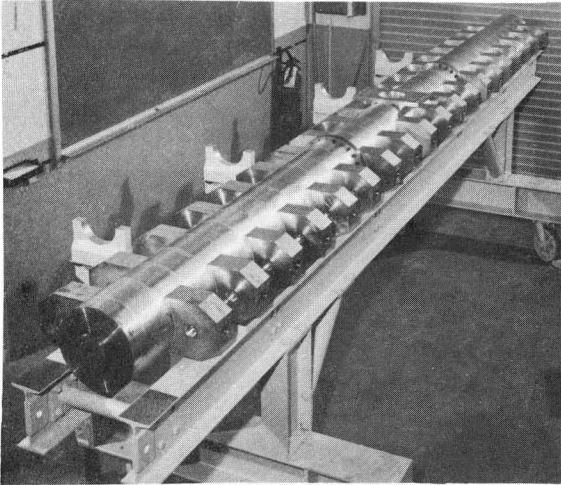


Fig. 1. A 39 accelerating cell, $\beta = 0.65$ side coupled cavity chain prior to final tuning and installation of vacuum and cooling systems.

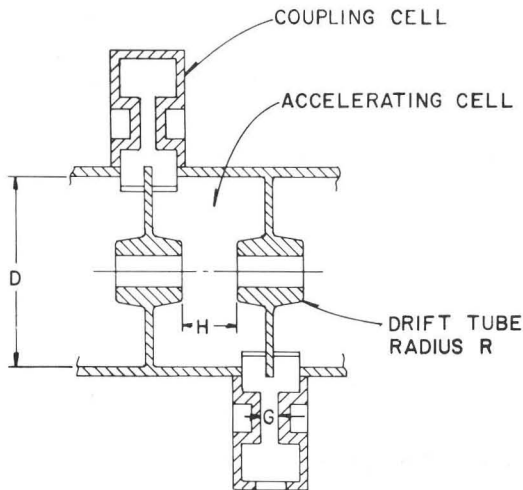


Fig. 2. Cross section of one accelerating cell and two coupling cells in a side coupled cavity chain.

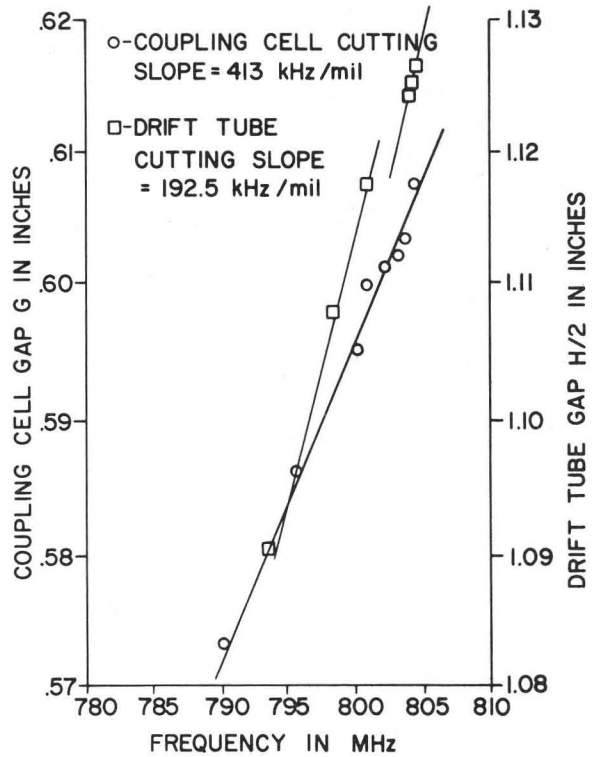


Fig. 3. The variation in cell frequency due to the dimensional change in gaps between accelerating cell drift tubes or coupling cell bosses.

SIDE COUPLED CAVITY DISPERSION RELATIONS

$$\omega^2 = \omega_1^2 (A) + \omega_2^2 (B) + \frac{2 [AB - K^2 \cos^2 \phi]}{[\omega_1^2 A + \omega_2^2 B]^2 - 4 \omega_1^2 \omega_2^2 [AB - K^2 \cos^2 \phi]}$$

K = CELL TO CELL COUPLING $K^1 = \textcircled{1}$ TO $\textcircled{1}$ COUPLING $K^2 = \textcircled{2}$ TO $\textcircled{2}$ COUPLING
 $A = 1 + K^1 \cos 2\phi$ $B = 1 + K^2 \cos 2\phi$

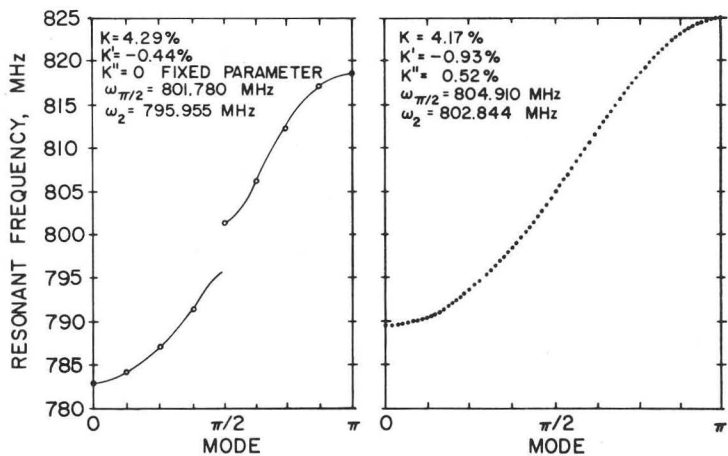


Fig. 4. Dispersion curves for a multi-cell system which illustrate the difference between an untuned and a tuned system.

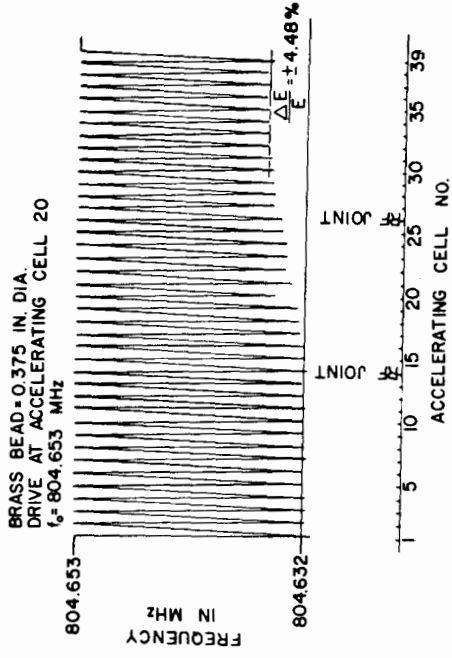


Fig. 7. The frequency perturbation in cavity chain due to round brass bead drawn down beam axis of tank prior to final tuning.

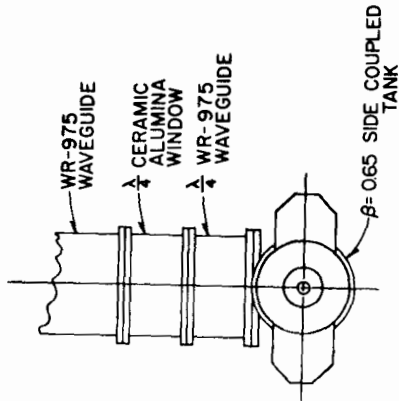


Fig. 6. Power is coupled into tank through aperture in accelerating cell 20.

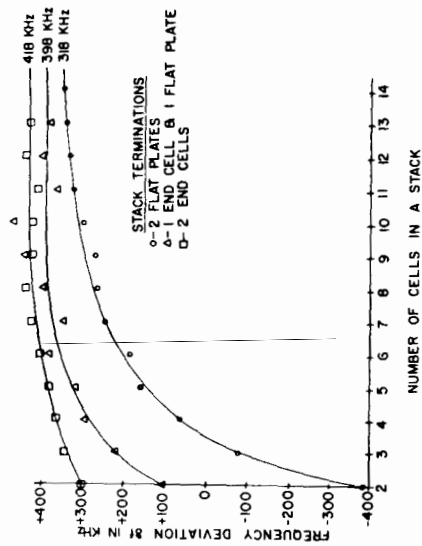


Fig. 5. Frequency deviation Δf as a function of number of cells in a stack.

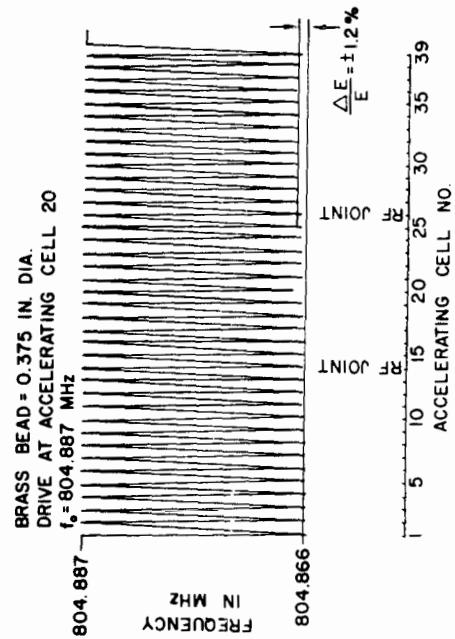


Fig. 8. Frequency perturbation in cavity chain due to round brass bead drawn down beam axis of tank after final tuning.

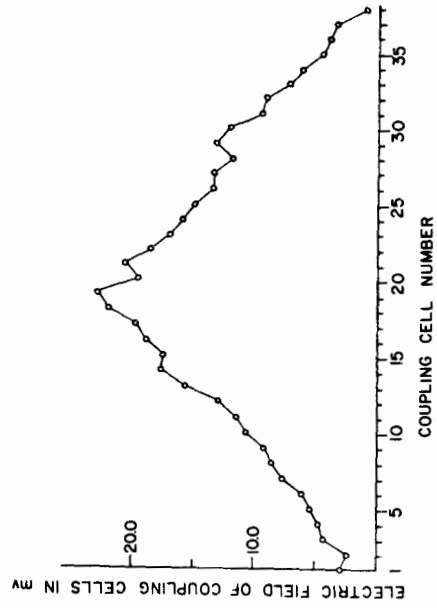


Fig. 9. Plot of electric field in coupling cells shows expected linear dependence on cell number.